Distributed spacing control for multiple, buoyancy-controlled underwater robots

Cong Wei[1][0000−0002−6552−7239] and Derek A. Paley[1,2][0000−0002−3086−2395]

[1] Institute for Systems Research, University of Maryland, College Park, MD 20742, USA
[2] Department of Aerospace Engineering, University of Maryland, College Park, MD 20742, USA
weicong,dpaley@umd.edu

Abstract. This paper presents a distributed coordination algorithm for multiple, buoyancy controlled underwater robots to achieve a moving formation in a shear flow. This work is motivated by the deployment of a swarm of ocean-going robots called Driftcam to observe the pelagic scattering layer. Driftcam horizontal motion is determined by the flow field and the vertical motion is regulated by the buoyancy control. Pairwise range measurements are available to the Driftcam network via acoustic transponders. A formation buoyancy controller is designed using the backstepping method; deviation from the desired formation is measured by a potential function. Numerical simulations illustrate the efficacy of the control algorithm and motivate ongoing and future efforts to estimate of the scattering layer density.

Keywords: Coordination · Formation Control · Underwater Robots

1 Introduction

The distributed control of multi-agent systems in the ocean is developing rapidly, motivated by the limitations of individual agents [15, 17], the scale of the spatial area needing coverage, and redundancy in the case of individual failure [5]. Due to the ocean's large-scale spatiotemporal patterns, it is advantageous to send a distributed sensor network for applications such as cooperative mine countermeasures [18] and search and recovery missions [7, 11]. One specific motivation that underpins the results of this paper is the deployment of ocean-going robots to perform oceanographic observation of ecosystem processes in the ocean that are critical indicators of climate change.

This paper addresses the problem of coordinating a distributed network of short-range interacting mobile underwater sensors. Called Driftcam, this robotic sensor is propelled by ocean currents and is used for counting and measuring organisms in the pelagic scattering layer using a high-definition low-light camera [16]. Multiple Driftcams have the capability to regulate their horizontal separation by adjusting their depth to take advantage of the vertical variation of flow speed in the ocean. Depth is regulated using a piston pump engine, which pumps oil into an external bladder that can change buoyancy by its expandable volume [2].

The pelagic scattering layer is an ecosystem consisting of marine organisms that undertake diel vertical migrations, swimming into deeper waters during daytime and

ascending toward the surface at night [4]. Because of the huge biomass involved, the migrations in the pelagic scattering layer account for the largest daily movement of biomass on this planet [4]. Although shipboard echosounders can count and measure specific species [10], they are insufficient to capture a panoramic view of the overall community structure and behavior [16]. Prior and ongoing work [16] presents a control strategy for a single Driftcam to track the scattering layer but does not consider how the flow influences the motion of the Driftcam. Preliminary field results have been obtained for deployments into the scattering layer in the Guaymas Basin of the Gulf of California, Mexico, showing the utility of the Driftcam system in the field [1–3]. A Driftcam formation estimates the local concentration of organisms by collecting in situ observations from discrete locations in the scattering layer. The challenge addressed in this paper is deriving a control strategy to stabilize a moving formation of multiple Driftcams with desired horizontal spacing.

Formation control is inspired by collective motion in groups of animals with local interactions [6]. The primary issue in an engineering application is how to design these interactions so that the agents converge to the desired group behavior [15]. One option to measure how the configuration of a swarm differs from the desired formation [12] is to use a potential function that is minimized by the desired formation. Such a function is also suitable for the design of a formation controller, since an energy-based representation is compatible with a Lyapunov-based control design. Since agent receives information from its neighbors within communication range, the design of the formation controller also relies on the communication topology, typically described using graph theory.

In this paper, the desired formation is achieved by designing a distributed depth controller. Since Driftcams can only directly regulate their depth, they must rely on the horizontal current at that depth to move them towards a desired formation [14]. The horizontal current is modeled as shear flow field whose speed decreases with depth. Backstepping [8] is invoked to map the controller design to a buoyancy input. The individual controller for each Driftcam tracks the time-varying reference depth of the scattering layer and converges to the desired formation using measurements of the range to its neighbors.

The contributions of this paper are (i) a distributed formation control strategy for a team of Driftcams in a shear flow based on a potential function that has a stable global minima when agents are equally spaced; and (ii) a backstepping approach to design a depth-tracking formation controller while achieving the desired formation. This paper provides a new perspective on taking advantage of environment flow fields to facilitate formation control for long-endurance multi-agent systems with limited onboard actuation. The result is tested in a simulated environment where a group of agents are released to achieve a horizontal formation with equal spacing while tracking the time-varying depth of the scattering layer.

The paper is structured as follows. Section 2 reviews the graph theory that is used to model the interaction of the group. Section 3 formulates the problem and outlines the key assumptions. The construction of the potential function is introduced in Section 4 along with the application of the backstepping method. Section 5 shows simulation results. Related ongoing and future work is summarized in Section 6.

2 Preliminaries

This section introduces several basic concepts from algebraic graph theory and robotic control via artificial potential functions. More details can be found in [12].

2.1 Graph theory

A graph $\mathcal{G} = (\mathcal{V}, \mathcal{E})$ is composed of a set of vertices $\mathcal{V} = \{1, 2, \cdots, n\}$ and edges $\mathcal{E} \subseteq \{(i, j)|i, j \in \mathcal{V}, i \neq j\}$. The interaction graph used in this paper is undirected, i.e., $(i, j) \in \mathcal{E} \Leftrightarrow (i, j) \in \mathcal{E}$. The set of neighbors of a node i in graph $\mathcal{G}$ is thus defined as

$$N_i = \{j \in \mathcal{V}|(i, j) \in \mathcal{E}\}.$$

The communication range between two agents is denoted by r. Neighbor $j \in N_i$ at distance d_{ij} from agent i in graph $\mathcal{G}$ can thus be represented by being within an open ball with radius r, i.e.,

$$N_i = \{j \in \mathcal{V}|d_{ij} \leq r\}.$$

Two nodes $i, j \in \mathcal{G}(x)$ are connected by a path if there exists a sequence of distinct nodes starting with i and ending with j such that consecutive nodes are neighbors [19].

2.2 Potential function

A smooth collective potential function is constructed as follows [12]. Let $\boldsymbol{\Xi} = [\xi_1, \xi_2, \cdots]^T,\ i, j \in \{1, \cdots, n\}$. Then

$$V(\boldsymbol{\Xi}) = \frac{1}{2}\sum_{i=1}^{n}\sum_{j\neq i, j=1}^{n} \psi_\alpha(\|\xi_j - \xi_i\|_\sigma), \tag{1}$$

where $\psi_\alpha(\xi)$ is a smooth pairwise attractive/repulsive potential with finite cut-off at $r_\alpha = \|r\|_\sigma$ and a global minimum at $\xi = d_\alpha$ defined as [12]

$$\psi_\alpha(\xi) = \int_{d_\alpha}^{\xi} \phi_\alpha(s)\mathrm{d}s. \tag{2}$$

The σ-norm of a vector is a map $\mathbb{R}^m \to \mathbb{R}^+$ defined as [12]

$$\|\xi\|_\sigma = \frac{1}{\epsilon}[\sqrt{1 + \epsilon\|\xi\|^2} - 1]. \tag{3}$$

The norm $\|\xi\|_\sigma$ is used rather than $\|\xi\|$ because the latter is not differentiable at $z = 0$ [12]. The action function $\phi_\alpha(\xi)$ is integrated to construct a smooth pairwise potential with finite cut-off vanishing for all $\xi \geq r_\alpha$.

In the following, we use

$$\phi_\alpha(\xi) = \rho_h(\xi/r_\alpha)\phi(\xi - d_\alpha) \tag{4}$$

$$\phi(\xi) = \frac{1}{2}[(a + b)\sigma_1(\xi + c) + (a - b)], \tag{5}$$

where $\sigma_1(\xi) = \xi/\sqrt{1+z^2}$ and $0 < a \leq b,\ c = |a-b|/\sqrt{4ab}$ to guarantee $\phi(0) = 0$. The bump function $\rho_h(\xi)$ is

$$\rho_h(\xi) = \begin{cases} 1, & \xi \in [0, h) \\ \frac{1}{2}[1 + \cos(\pi \frac{\xi - h}{1-h})], & \xi \in [h, 1] \\ 0 & \text{otherwise.} \end{cases} \tag{6}$$

Remark 1. The bump function $\rho_h(\xi)$ ensures the function $V(\xi)$ is smooth for any configuration of $\mathcal{G}$.

3 Problem formulation

Driftcam behaves as a submersible buoy drifting in the ocean, unattached to the ocean floor or a boat; it changes depth by controlling its buoyancy. The vehicle's vertical motion is subject to hydrodynamic drag proportional to drag coefficient b_d [16]. Assume that the drifter's horizontal velocity is equal to the ocean's horizontal velocity at its current location. Let $\mathbf{x} = [x_1, x_2, \cdots, x_n]^T$ and $\mathbf{z} = [z_1, z_2, \cdots, z_n]^T$ represent the Driftcam horizontal and vertical positions, respectively. The collective dynamics are [16]

$$\dot{x} = v = f(z) \tag{7a}$$

$$\ddot{z} = \mathrm{sat}(\mu, \mu_{\max}) - b_d \mathrm{diag}\{\dot{z}\}|\dot{z}|, \tag{7b}$$

where $\mu = \mu(x, z, \dot{z}) \in \mathbb{R}^n$ represents the difference between the Driftcam's weighted buoyancy; $\mathrm{diag}\{\dot{z}\}$ is a diagonal matrix with each entry on the diagonal being $\dot{z}_i$. The saturation term denotes the drifter's maximum vertical force $\mu_{\max}$. Consider a priori known shear flow $f(z)$ with constant slope, i.e., $f(z) = Az + B, A, B \in \mathbb{R}$. Because of our choice of reference, this flow model does not produce motion in the vertical direction and depends continuously on depth [13,14] The scattering layer nominal depth $\zeta(t)$ obeys

$$\ddot{\zeta} = -\omega^2(\zeta - \zeta(0)),\ \omega \in \mathbb{R}.$$

For Driftcam i, let $w_i = \dot{z}_i$ and assume $\mu < \mu_{\max}$. We have the following dynamics

$$\dot{x}_i = Az_i + B \tag{8a}$$

$$\dot{z}_i = w_i \tag{8b}$$

$$\dot{w}_i = \mu_i - b_d \dot{z}_i|\dot{z}_i| \triangleq u_i. \tag{8c}$$

Assume graph $\mathcal{G}$ consisting of agents $\mathcal{V} = \{1, 2, \ldots, n\}$ and edges $\mathcal{E} \subseteq \{(i,j)|i,j \in \mathcal{V}, j \neq i\}$ is initially connected. The goal for an initially connected group of n Driftcams with communication range $r \in \mathbb{R}$ is to converge to a equally spaced formation tracking the nominal depth $\zeta(t)$ of scattering layer. Mathematically, the goal is

$$\|x_i(t) - x_j(t)\| \to d,\ d \in \mathbb{R} \tag{9a}$$

$$z_i(t) = z_j(t) \to \zeta(t),\ \forall\, i \in N_j, i = 1, \cdots, n. \tag{9b}$$

4 Technical Approach

A collective potential function is constructed to generate the desired vertical velocity w_i and then backstepping is applied to derive the buoyancy control u_i, for all agents $i = 1, \cdots, n$.

4.1 Construction of potential function

The Driftcam move with the flow in the horizontal direction. Motivated by objective (9a), a smooth pairwise collective potential is constructed using the horizontal position differences in the form $\|x_j - x_i\|_\sigma$, i.e.,

$$V(x) = \tfrac{1}{2} \sum_{i=1}^{n} \sum_{j \neq i, j=1}^{n} \psi_\alpha(\|x_j - x_i\|_\sigma). \tag{10}$$

Remark 2. As shown in (4), if $\|x_j - x_i\|_\sigma > \|r\|_\sigma$, the corresponding potential for i and j diminishes. So the second summation in (10) is over the neighbors of agent i.

The following design of w_i is proposed:

$$w_i = \sum_{j \in N_i} \phi_\alpha(\|x_j - x_i\|_\sigma) n_{ij} + f_i^\gamma(z_i, \zeta, \dot{\zeta}), \tag{11}$$

where the first term is the gradient of (1) and $n_{ij} = \frac{x_j - x_i}{\sqrt{1 + \epsilon \|x_j - x_i\|^2}}$. $f_i^\gamma(z_i, \zeta, \dot{\zeta})$ is the navigational feedback given by

$$f_i^\gamma(z_i, \zeta, \dot{\zeta}) = -c_1(z_i - \zeta) + \dot{\zeta}\,, c_1 > 0. \tag{12}$$

Stacking $w_i, i = \{1, \cdots, n\}$, together, we can get

$$w = -\nabla V(p) + f^\gamma(z, \zeta, \dot{\zeta}). \tag{13}$$

Now consider a moving frame C that is centered at $[x_c(t), z_c(t)]^{\mathrm{T}}$, the mass center of all agents, i.e., $x_c = 1/n \sum_{i=1}^{n} x_i$ and $z_c = 1/n \sum_{i=1}^{n} z_i$. The position of agent i in C is

$$p_i = x_i - x_c \tag{14a}$$

$$q_i = z_i - z_c. \tag{14b}$$

It can be shown that $V(x) = V(p)$. The convergence proof needs a decomposition lemma, following [12].

Lemma 1. *Let*

$$[g_1, \cdots, g_n]^T = g(q) = -c_1 q \tag{15a}$$

$$h(z_c, \zeta, \dot{\zeta}) = -c_1(z_c - \zeta) + \dot{\zeta}. \tag{15b}$$

Suppose the navigation feedback $f_i^{\gamma}(z_i, \zeta, \dot{\zeta})$ *in* (12) *is linear, i.e., there exists a decomposition of* $f_i^{\gamma}(z_i, \zeta, \dot{\zeta})$ *in the following form:*

$$f_i^{\gamma}(z_i, \zeta, \dot{\zeta}) = g_i(q_i) + h(z_c, \zeta, \dot{\zeta}). \tag{16}$$

Then, applying (13)*, system* (8a) *and* (8b) *can be decomposed into a second-order system,*

$$\dot{p} = Aq, \tag{17a}$$
$$\dot{q} = -\nabla V(p) + g(q), \tag{17b}$$

and another second-order system in frame C*,*

$$\dot{x}_c = Az_c + B, \tag{18a}$$
$$\dot{z}_c = h(z_c, \zeta, \dot{\zeta}). \tag{18b}$$

The system (17) describes the structural dynamics and (18) is the translational dynamics [12]. The depth convergence (8b) can be proved by applying feedback controller (15b) to (18) if $c_1 > 0$. The following theorem shows how (9a) is achieved from (17).

Theorem 1. *Consider a group of agents with dynamics* (17) *and assume the initial structural energy* (10) *of those agents is less than* $(k+1)c^*$ *with* $c^* = \psi_\alpha(0),\ k \in \mathbb{Z}_+$*. The goal* (9a) *is achieved asymptotically and at most k distinct pairs of agents collide, where* $k = 0$ *implies collision-free motion.*

Proof. The Hamiltonian of the structural dynamics (17) is chosen as a Lyapunov candidate function:

$$H(p, q) = V(p) + \tfrac{1}{2} q^T q. \tag{19}$$

Taking the derivative of (19) along solutions of (17) yields

$$\dot{H}(p, q) = -c_1 q^{\mathrm{T}} q \leq 0. \tag{20}$$

By LaSalle's invariance principle, all solutions converge to the largest invariant set in $E = \{(p, q) | \dot{H} = 0\}$. Based on (20), the velocity of all the agents match the velocity of the moving frame, i.e., $q \equiv 0$. At the same time, it implies that $V(p)$ converges to the minimum asymptotically, which implies $\|p_j - p_i\|_\sigma \to d_\sigma \Leftrightarrow |x_j - x_i| \to d$.

Collision-free motion can be proved by contradiction. Suppose there are at least $k+1$ agents colliding at time $t_1 \geq t_0$, which implies

$$V(p(t_0)) \geq V(p(t_1)) \geq (k+1)\psi_\alpha(0). \tag{21}$$

However, (21) contradicts the fact that

$$V(p(t_0)) \leq H(t_0) < (k+1)\psi_\alpha(0).$$

Therefore, at most k pairs collide and, when $k = 0$, there are no colliding pairs.

To give the initial condition more explicitly, let $k = 1$. In this case,

$$V(p(0)) = V(x(0)) = \tfrac{1}{2}\sum_{i=1}^{n}\sum_{j\neq i,j=1}^{n}\psi_\alpha(\|x_j - x_i\|_\sigma) \leq \psi_\alpha(0),$$

where

$$\begin{aligned}\psi_\alpha(0) &= \int_{d_\alpha}^{0}\phi_\alpha(s)\mathrm{d}s = -\int_{0}^{d_\alpha}\rho_h(s/r_\alpha)\phi(s-d_\alpha)\mathrm{d}s \overset{a=b}{=} -a\int_{0}^{d_\alpha}\rho_h(s/r_\alpha)\sigma_1(s-d_\alpha)\mathrm{d}s \\ &= -a\int_{0}^{d_\alpha}\rho_h(s/r_\alpha)\tfrac{s-d_\alpha}{\sqrt{1+(s-d_\alpha)^2}}\mathrm{d}s \geq \delta a\int_{0}^{d_\alpha}\tfrac{d_\alpha-s}{\sqrt{1+(d_\alpha-s)^2}}\mathrm{d}s = \delta a(\sqrt{1+d_\alpha}-1).\end{aligned}$$

A collision-free formation requires the initial structural energy to satisfy $V(x(0)) \leq \delta a(\sqrt{1+d_\alpha}-1)$. □

4.2 Backstepping Controller design

Controller design for extended structural dynamics The controller u is designed through backstepping based on system (17).

Theorem 2. *Let $y = w - \dot{z}_c$. Consider the extended structural dynamics,*

$$\dot{p} = Aq \tag{22a}$$
$$\dot{q} = y \tag{22b}$$
$$\dot{y} = \nu \tag{22c}$$

under control input

$$\nu = -A\nabla^2 V(p)q - (c_1+c_2)y - c_2\nabla V(p) - (c_1c_2+1)q. \tag{23}$$

Then $y \to \eta(p,q) \triangleq -\nabla V(p) + g(q)$ asymptotically.

Proof. Based on (17) and

$$\gamma(p,q) = y - \eta(p,q),$$

we can transform (22) into

$$\dot{p} = Aq \tag{24a}$$
$$\dot{q} = \eta(p,q) + y - \eta(p,q) = \eta(p,q) + \gamma \tag{24b}$$
$$\dot{\gamma} = \nu - \dot{\eta}(p,q) = \tilde{\nu}. \tag{24c}$$

Consider Lyapunov candidate

$$V_c = H(p,q) + \tfrac{1}{2}\gamma^T\gamma.$$

Whose derivative is

$$\dot{V}_c = -c_1 q^T q + \gamma^T q + \gamma^T\tilde{\nu}. \tag{25}$$

Let

$$\tilde{\nu} = -c_2\gamma - q,$$

such that

$$\dot{V}_c = -c_1 q^T q - c_2 \gamma^T \gamma. \tag{26}$$

Therefore

$$\nu = \dot{\gamma}(p,q) - c_2(y - \gamma(p,q)) - q,$$

which leads to (23). □

Controller design for extended translational dynamics Since the depth tracking for the translational dynamics is not related to (18a), extending (18b) yields

$$\dot{z}_c = y_c \tag{27a}$$
$$\dot{y}_c = \nu_c. \tag{27b}$$

Theorem 3. *Consider* (27) *with control input*

$$\nu_c = -(1+c_1)(z_c - \zeta) - (1+c_1)(y_c - \dot{\zeta}) + \ddot{\zeta}. \tag{28}$$

Then $y_c \to \eta_c(z_c, \zeta, \dot{\zeta}) \triangleq -c_1(z_c - \zeta) + \dot{\zeta}$ *asymptotically.*

Proof. Let $\tilde{y}_c = y_c - \eta_c$, so (27) implies

$$\dot{z}_c = \eta_c + \tilde{y}_c \tag{29a}$$
$$\dot{\tilde{y}}_c = \nu_c - \dot{\eta}_c = \tilde{\nu}_c. \tag{29b}$$

Lyapunov candidate

$$V_e = \tfrac{1}{2}(z_c - \zeta)^2 + \tfrac{1}{2}\tilde{y}_c^2.$$

has time derivative

$$\dot{V}_e = (z_c - \zeta)(\dot{z}_c - \dot{\zeta}) + \tilde{y}_c\tilde{\nu}_c = -(z_c - \zeta)^2 + \tilde{y}_c(\tilde{\nu}_c + z_c - \zeta).$$

Taking

$$\nu_c = \dot{\eta}_c - \tilde{y}_c - (z_c - \zeta) \tag{30}$$

yields $\dot{V}_c = -(z_c - \zeta)^2 - \tilde{y}_c^2 \leq 0$. □

Combining (23) and (28), the net buoyancy control is

$$\mu = u + b_d \mathrm{diag}\{\dot{z}\}|\dot{z}| = \nu + \nu_c + b_d \mathrm{diag}\{\dot{z}\}|\dot{z}|. \tag{31}$$

As a result, to achieve formation control, each agent i needs to know the range (for constructing $\nabla V(p)$) of all of its neighbors $j \in N_i$, the dynamics of the scattering layer, and the mass center of all Driftcams.

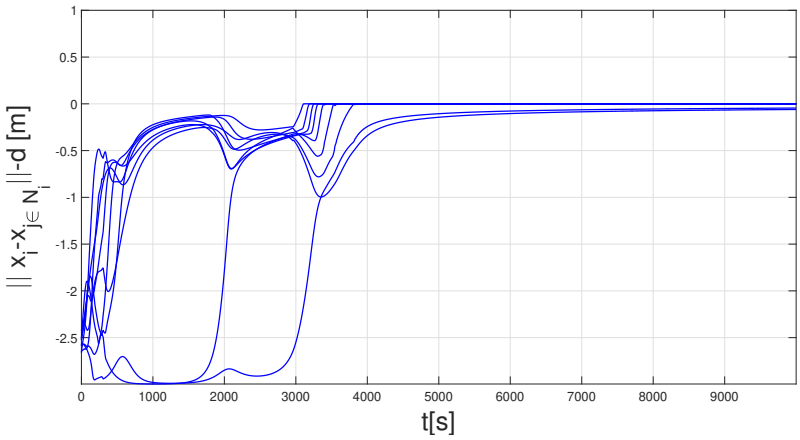

(a) The distances between neighbors of the Driftcams converge to the desired range d.

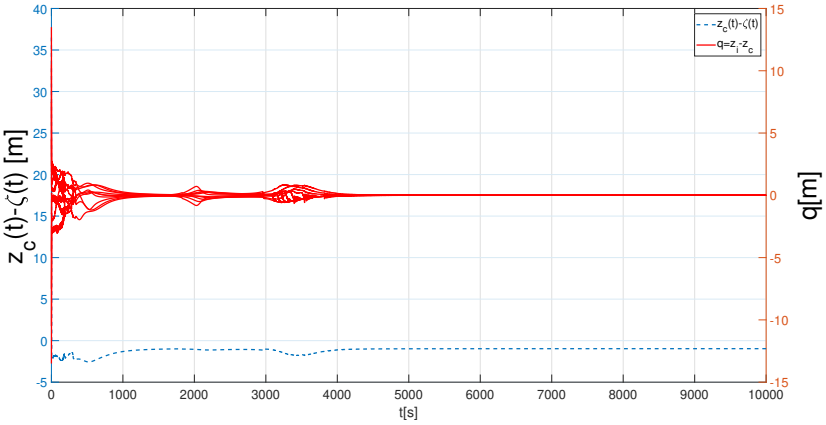

(b) Each Driftcam succeeds in tracking the depth of the swarm mass center $z_c(t)$ and the scattering layer's nominal depth $\zeta(t)$, which varies sinusoidally in depth.

Fig. 1. Simulation results for a Driftcam formulation tracking a time-varying scattering layer.

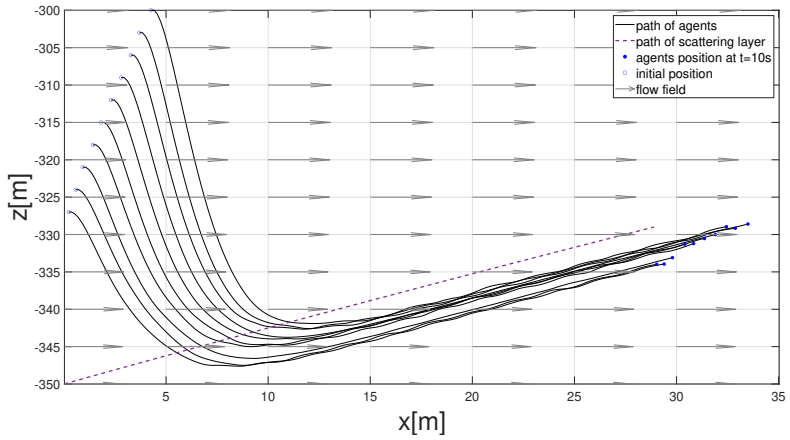

(a) Path of the swarm from $t = 0s$ to $t = 10s$.

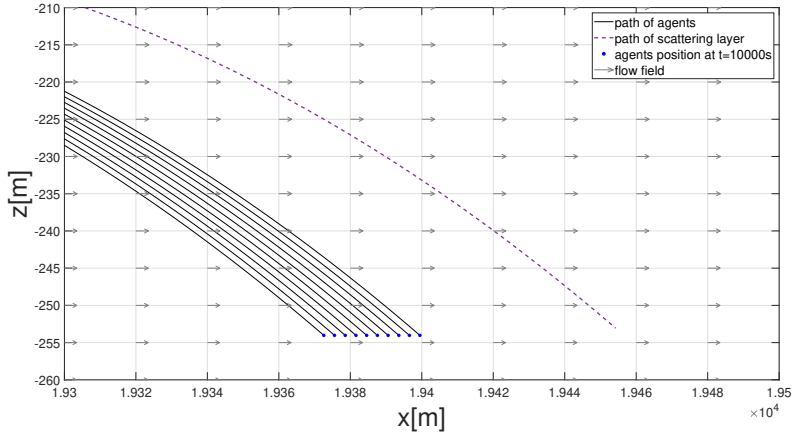

(b) Path from $t = 9900s$ to $t = 10000s$.

Fig. 2. Path of agents and scattering layer. The length of the gray arrows denotes the flow speed.

5 Simulation Results

The following simulations illustrate the performance of the control strategy designed to achieve equal spacing and depth tracking for a group of Driftcams. The parameters for potential function (10) are as follows: $d = 3m$, $r = d$, $\epsilon = 0.1$, $a = b = 5$, and $h = 0.2$. The parameters for controller (31) are $c_1 = 3.5$, $c_2 = 1$, and $b_d = 0.1/m$. The parameters for the shear flow are $A = 0.0062/s$ and $B = 5m/s$. The nominal depth of the scattering layer, which is the reference depth signal, is chosen to be [9].

$$\zeta(t) = A_\omega \sin(\omega t + \phi) + \zeta(0),$$

where $A_\omega = 300m,\ \omega = 1/120rad,\ \phi = \pi/6,$ and $\zeta(0) = -500m$.

Ten Driftcam are initially released within communication range using $[x_i(0), z_i(0)] \in [0, 4] \times [-330, -300]$. The simulation runs for $t = 10000s$. Figure 1(a) illustrates how the distance error between neighbors converges to the desired value d. The tracking performance is presented in Figure 1(b). The process of convergence in the horizontal direction is not monotonic since the horizontal error tuning in one pair may be transmitted to another one several hops away. Balancing horizontal tuning and vertical tracking is the subject of ongoing and future work. Compared with the formation from $t = 0s$ to $t = 10s$ and $t = 9900s$ to $t = 10000s$, the initial configuration in Fig. 2(a) is gradually transformed into the formation with equal distancing in Fig. 2(b) while achieving the depth tracking. The whole picture is shown in Fig. 3.

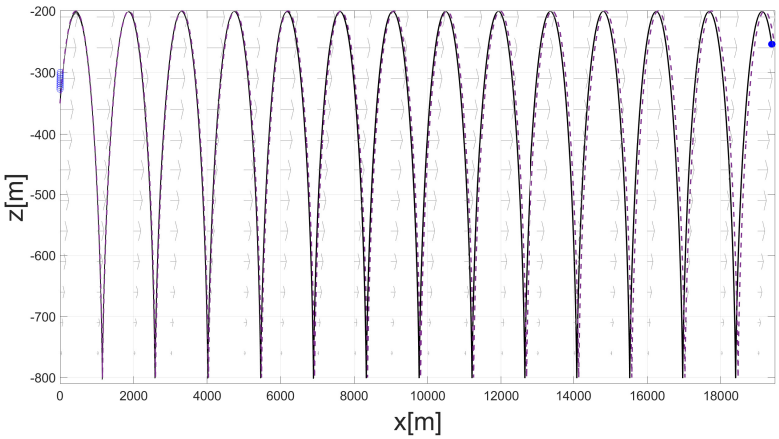

Fig. 3. Path of agents from $t = 0$ to $t = 10000$.

6 Conclusion

This paper presents a formation strategy for a moving network of underwater robotic sensors in a shear flow field. The buoyancy-driven Driftcam is modeled as an underactuated system. A depth controller is designed to track the scattering layer and achieve equal spacing between neighbors in a Driftcam formation. The formation strategy is built on a potential function that measure the deviation energy of the swarm's configuration from the desired formation. Backstepping is applied for controlling the dynamics and LaSalle's invariance principle is used to establish the stability for the moving formation described in a moving frame. Simulation results motivate the need to balance depth tracking and horizontal spacing, since once the former is done it is more difficult for the latter to be executed.

In ongoing work, a recursive filter is used to estimate the horizontal shear flow from pairwise range measurements. Another objective is to estimate the density of the

scatter layer using onboard measurements of the organism density. Together with the presented formation strategy, the Driftcam sensor network can be adapted according to the exploration requirements.

References

1. Berkenpas, E.J., Henning, B.S., Shepard, C.M., Turchik, A.J.: The driftcam: A buoyancy controlled pelagic camera trap. In: 2013 OCEANS - San Diego. pp. 1–6 (2013). https://doi.org/10.23919/OCEANS.2013.6741018
2. Berkenpas, E.J., Henning, B.S., Shepard, C.M., Turchik, A.J., Robinson, C.J., Portner, E.J., Li, D.H., Daniel, P.C., Gilly, W.F.: A buoyancy-controlled Lagrangian camera platform for *In Situ* imaging of marine organisms in midwater scattering layers. IEEE Journal of Oceanic Engineering **43**(3), 595–607 (2018). https://doi.org/10.1109/JOE.2017.2736138
3. Berkenpas, E.J., Shepard, C.M., Suitor, R., Zaidins, P., Paley, D., Abernathy, K.: Swarming driftcams: a novel platform for locating and tracking pelagic scattering layers. In: OCEANS 2021: San Diego – Porto. pp. 1–6 (2021). https://doi.org/10.23919/OCEANS44145.2021.9705972
4. Brodeur, R., Pakhomov, E.: Nekton. In: Cochran, J.K., Bokuniewicz, H.J., Yager, P.L. (eds.) Encyclopedia of Ocean Sciences (Third Edition), pp. 582–587. Academic Press, Oxford (2019). https://doi.org/https://doi.org/10.1016/B978-0-12-409548-9.11460-5
5. Cortés, J., Egerstedt, M.: Coordinated control of multi-robot systems: A survey. SICE Journal of Control, Measurement, and System Integration **10**(6), 495–503 (2017). https://doi.org/10.9746/jcmsi.10.495
6. Gautrais, J., Ginelli, F., Fournier, R., Blanco, S., Soria, M., Chaté, H., Theraulaz, G.: Deciphering interactions in moving animal groups. PLOS Computational Biology **8**(9), 1–11 (09 2012). https://doi.org/10.1371/journal.pcbi.1002678
7. Kemna, S., Caron, D.A., Sukhatme, G.S.: Constraint-induced formation switching for adaptive environmental sampling. In: Proceedings of the MTS/IEEE OCEANS 2015. pp. 1–7 (2015)
8. Khalil, H.K.: Nonlinear systems. Prentice Hall (2002)
9. Knutsen, T., Wiebe, P.H., Gjøsæter, H., Ingvaldsen, R.B., Lien, G.: High latitude epipelagic and mesopelagic scattering layers—a reference for future arctic ecosystem change. Frontiers in Marine Science **4** (2017). https://doi.org/10.3389/fmars.2017.00334
10. Lavery, A.C., Chu, D., Moum, J.N.: Measurements of acoustic scattering from zooplankton and oceanic microstructure using a broadband echosounder. ICES Journal of Marine Science **67**(2), 379–394 (10 2009). https://doi.org/10.1093/icesjms/fsp242
11. Meghjani, M., Shkurti, F., Higuera, J.C.G., Kalmbach, A., Whitney, D., Dudek, G.: Asymmetric rendezvous search at sea. In: Proceedings of the Canadian Conference on Computer and Robot Vision. pp. 175–180 (2014)
12. Olfati-Saber, R.: Flocking for multi-agent dynamic systems: algorithms and theory. IEEE Transactions on Automatic Control **51**(3), 401–420 (2006). https://doi.org/10.1109/TAC.2005.864190
13. Ouimet, M., Cortes, J.: Robust, distributed estimation of internal wave parameters via interdrogue measurements. IEEE Transactions on Control Systems Technology **22**(3), 980–994 (2014). https://doi.org/10.1109/TCST.2013.2270952
14. Ouimet, M., Cortés, J.: Coordinated rendezvous of underwater drifters in ocean internal waves. In: 53rd IEEE Conference on Decision and Control. pp. 6099–6104 (2014). https://doi.org/10.1109/CDC.2014.7040344

15. Sepulchre, R., Paley, D.A., Leonard, N.E.: Stabilization of planar collective motion: All-to-all communication. IEEE Transactions on Automatic Control **53**(5), 811–824 (2007). https://doi.org/10.1109/TAC.2007.898077
16. Suitor, R., Berkenpas, E., Shepard, C.M., Abernathy, K., Paley, D.A.: Dynamics and control of a buoyancy-driven underwater vehicle for estimating and tracking the scattering layer. In: Preparation
17. Wei, C., Tanner, H.G.: Synchronization of geophysically-driven oscillators with short-range interaction. IEEE Transactions on Automatic Control pp. 1–1 (2021). https://doi.org/10.1109/TAC.2021.3058960
18. Yordanova, V., Griffiths, H.: Synchronous rendezvous technique for multi-vehicle mine countermeasure operations. In: Proceedings of the MTS/IEEE OCEANS 2015. pp. 1–6 (2015)
19. Zavlanos, M., Pappas, G.: Controlling connectivity of dynamic graphs. In: Proceedings of the 44th IEEE Conference on Decision and Control. pp. 6388–6393 (2005). https://doi.org/10.1109/CDC.2005.1583186